

1 Atmospheric $\Delta^{17}\text{O}(\text{NO}_3^-)$ reveals nocturnal chemistry dominates nitrate production 2 in Beijing haze

3 Pengzhen He¹, Zhouqing Xie^{1,2,3*}, Xiyuan Chi¹, Xiawei Yu¹, Shidong Fan¹, Hui Kang¹, Cheng Liu^{1,2,3}, Haicong Zhan¹

4 ¹Anhui Province Key Laboratory of Polar Environment and Global Change, School of Earth and Space Sciences, University
5 of Science and Technology of China, Hefei, Anhui 230026, China.

6 ²Center for Excellence in Urban Atmospheric Environment, Institute of Urban Environment, Chinese Academy of Sciences,
7 Xiamen, Fujian 361021, China.

8 ³Key Lab of Environmental Optics and Technology, Anhui Institute of Optics and Fine Mechanics, Chinese Academy of
9 Sciences, Hefei, Anhui 230031, China.

10

11 *Corresponding to: Zhouqing Xie (zqxie@ustc.edu.cn)

12

13 **Abstract.** The rapid mass increase of atmospheric nitrate is a critical driving force for the occurrence of fine-particle
14 pollution (referred to as haze hereafter) in Beijing. However, the exact mechanisms for this rapid increase of nitrate mass has
15 been not well constrained from field observations. Here we present the first observations of the oxygen-17 excess of
16 atmospheric nitrate ($\Delta^{17}\text{O}(\text{NO}_3^-)$) collected in Beijing haze to reveal the relative importance of different nitrate formation
17 pathways, and we also present the simultaneously observed $\delta^{15}\text{N}(\text{NO}_3^-)$. During our sampling period, 12h-averaged mass
18 concentrations of $\text{PM}_{2.5}$ varied from 16 to 323 $\mu\text{g m}^{-3}$ with a mean of $(141 \pm 88 \text{ (1SD)}) \mu\text{g m}^{-3}$, with nitrate ranging from 0.3
19 to 106.7 $\mu\text{g m}^{-3}$. The observed $\Delta^{17}\text{O}(\text{NO}_3^-)$ ranged from 27.5 ‰ to 33.9 ‰ with a mean of $(30.6 \pm 1.8) \text{‰}$ while $\delta^{15}\text{N}(\text{NO}_3^-)$
20 ranged from -2.5‰ to 19.2 ‰ with a mean of $(7.4 \pm 6.8) \text{‰}$. $\Delta^{17}\text{O}(\text{NO}_3^-)$ -constrained calculations suggest nocturnal
21 pathways ($\text{N}_2\text{O}_5 + \text{H}_2\text{O}/\text{Cl}^-$ and $\text{NO}_3 + \text{HC}$) dominated nitrate production during polluted days ($\text{PM}_{2.5} \geq 75 \mu\text{g m}^{-3}$) with the
22 mean possible fraction of 56 – 97 %. Our results illustrate the potentiality of $\Delta^{17}\text{O}$ in tracing nitrate formation pathways,
23 future modelling work with the constraint of isotope data reported here may further improve our understanding of nitrogen
24 cycle during haze.

25 1 Introduction

26 Severe and frequent haze pollution has become a crucial threat for the air quality in megacity Beijing and the North
27 China Plain in recent years. The high concentrations of $\text{PM}_{2.5}$ (particulate matter with an aerodynamic diameter equal or
28 less than 2.5 μm) during severe haze, of which the hourly average can reach 1000 $\mu\text{g m}^{-3}$ (Zheng et al., 2015a), is harmful

29 to the public health by contributing to cardiovascular morbidity and mortality (Cheng et al., 2013; Brook et al., 2010).
30 Nitrate is an important component of PM_{2.5}, accounting for 1–45 % of PM_{2.5} mass in Beijing and North China Plain (Wen et
31 al., 2015; Zheng et al., 2015a; Zheng et al., 2015b). The main formation pathways of atmospheric nitrate, **defined herein as**
32 **gas-phase HNO₃ plus particulate NO₃⁻**, in urban area are summarized in Fig. 1, which includes: (i) NO₂ oxidation by OH
33 radical in the gas-phase, (ii) heterogeneous uptake of NO₂ on wet aerosols, (iii) NO₃ radical reacting with hydrocarbon (HC),
34 and (iv) heterogeneous uptake of N₂O₅ on wet aerosols and chlorine-containing aerosols. Since OH radical is mainly present
35 in the daytime while NO₃ radical and N₂O₅ are mainly present in the nocturnal atmosphere (Brown and Stutz, 2012), NO₂ +
36 OH is usually referred as the daytime nitrate formation pathway while N₂O₅ + H₂O/Cl⁻ and NO₃ + HC are referred as
37 nocturnal formation pathways (Vicars et al., 2013; Sofen et al., 2014). During haze in Beijing, the mixing ratio of daytime
38 OH is modelled to be low (Zheng et al., 2015b; Rao et al., 2016) while relatively high mixing ratio of nocturnal N₂O₅ is
39 observed in several studies (Wang et al., 2017a; Li et al., 2018; Wang et al., 2017b), therefore, nocturnal pathways are
40 suggested to be most responsible for the high concentrations of atmospheric nitrate during haze (Su et al., 2017; Pathak et al.,
41 2009; Pathak et al., 2011). In addition, the high PM_{2.5} concentration and relative humidity during haze in Beijing favors
42 heterogeneous reactions, which renders NO₂ + H₂O being a potentially significant pathway for nitrate production (Wang et
43 al., 2017d; Tong et al., 2015; Zheng et al., 2015a).

44 Nitrogen isotopic composition of nitrate ($\delta^{15}\text{N}(\text{NO}_3^-)$, wherein $\delta^{15}\text{N} = (R_{\text{sample}}/R_{\text{reference}} - 1)$ with R representing isotope
45 ratios of ¹⁵N/¹⁴N in the sample and the reference atmospheric N₂) is useful in tracing source of its precursor NO_x (Xiao et al.,
46 2015; Beyn et al., 2014; Fang et al., 2011; Hastings et al., 2013). Anthropogenic sources of NO_x such as coal combustion are
47 generally enriched in $\delta^{15}\text{N}$ while natural NO_x sources such as soil emissions or lightning typically have negative or zero $\delta^{15}\text{N}$
48 signature (Hoering, 1957; Yu and Elliott, 2017; Felix et al., 2012). Therefore highly positive values of observed $\delta^{15}\text{N}(\text{NO}_3^-)$
49 can be considered as an indicator of anthropogenic combustion (Elliott et al., 2009; Fang et al., 2011), although this
50 judgment may be influenced by isotopic exchange between NO and NO₂ (Freyer et al., 1993; Walters et al., 2016), isotopic
51 fractionations associated with nitrate formation pathways and isotopic effects occurring during transport, such as deposition
52 of NO₃⁻ and HNO₃ partitioning between gas and particle phase (Freyer, 1991; Geng et al., 2014). The oxygen-17 excess
53 ($\Delta^{17}\text{O}$) of nitrate, defined as $\Delta^{17}\text{O} = \delta^{17}\text{O} - 0.52\delta^{18}\text{O}$, wherein $\delta^{\text{X}}\text{O} = (R_{\text{sample}}/R_{\text{reference}} - 1)$ with R representing isotope ratios
54 of ^XO/¹⁶O in the sample and the reference Vienna Standard Mean Ocean Water and X = 17 or 18, is particularly useful in
55 reflecting nitrate formation pathways (Michalski et al., 2003). Atmospheric nitrate from nocturnal reaction pathways has
56 higher $\Delta^{17}\text{O}$ than that from daytime OH oxidation at given $\Delta^{17}\text{O}(\text{NO}_2)$ (Table 1). And once formed, atmospheric $\Delta^{17}\text{O}(\text{NO}_3^-)$
57 cannot be altered by mass-dependent processes such as deposition during transport (Brenninkmeijer et al., 2003). Previous
58 studies have shown the utility of atmospheric $\Delta^{17}\text{O}(\text{NO}_3^-)$ in quantifying the relative importance of various nitrate formation
59 pathways (Alexander et al., 2009; Michalski et al., 2003; Patris et al., 2007; Savarino et al., 2013; Vicars et al., 2013). For
60 example, $\Delta^{17}\text{O}(\text{NO}_3^-)$ -constrained box modeling work of Michalski et al. (2003) suggests that more than 90 % of

61 atmospheric nitrate is from nocturnal $\text{N}_2\text{O}_5 + \text{H}_2\text{O}$ pathway in winter La Jolla, California, which is reflected by the highest
62 $\Delta^{17}\text{O}(\text{NO}_3^-)$ values being observed in winter. In another study, Alexander et al. (2009) use observed $\Delta^{17}\text{O}(\text{NO}_3^-)$ to constrain
63 3D model and found that daytime $\text{NO}_2 + \text{OH}$ pathway dominates global tropospheric nitrate production with an annual mean
64 contribution of 76 %.

65 Until now, however, field observations of atmospheric $\Delta^{17}\text{O}(\text{NO}_3^-)$ have not been conducted in north China to constrain
66 the relative importance of different nitrate formation pathways during haze. In this work, we present the first observations of
67 atmospheric $\Delta^{17}\text{O}(\text{NO}_3^-)$ during Beijing haze from October 2014 to January 2015, and use this observation to examine the
68 importance of nocturnal formation pathways. We also present the signature of simultaneously observed $\delta^{15}\text{N}(\text{NO}_3^-)$.

69 **2 Materials and Methods**

70 **2.1 Sampling and atmospheric observations**

71 $\text{PM}_{2.5}$ filter samples were collected at a flow rate of $1.05 \text{ m}^3 \text{ min}^{-1}$ by a high volume air sampler (model TH-1000C II,
72 Tianhong Instruments Co., Ltd, China). The filter is quartz microfiber filter (Whatman Inc., UK), pre-combusted at 450°C
73 for 4 h before sampling. Our sampling period lasted from October 2014 to January 2015 with the collection interval being 12
74 h (08:00 – 20:00 LT or 20:00 – 08:00 LT) for each sample. Blank control samples were also collected. The blank was
75 sampled identically to the real sample except that the collection interval is 1 min. Due to that gaseous HNO_3 is likely to
76 adsorb onto particulate matter already trapped by the filter material (Vicars et al., 2013), the nitrate species collected is likely
77 to include both particulate nitrate and gaseous HNO_3 , which is referred to as atmospheric nitrate in previous studies (Vicars
78 et al., 2013; Morin et al., 2009; Michalski et al., 2003) and in this study. The sampling site is at the campus of University of
79 the Chinese Academy of Sciences (40.41°N , 116.68°E , $\sim 20 \text{ m}$ high) in suburban Beijing, about 60 km northeast of
80 downtown (Fig. 2), which is a super site set by HOPE-J³A (Haze Observation Project Especially for Jing-Jin-Ji Area) with
81 various observations being reported (Zhang et al., 2017; Xu et al., 2016; Chen et al., 2015; Tong et al., 2015; He et al., 2018).
82 Hourly concentrations of surface $\text{PM}_{2.5}$, CO , SO_2 , NO_2 and O_3 were observed at Huairou station (40.33°N , 116.63°E) by
83 Beijing Municipal Environmental Monitoring Center, about 10 km to our sampling site. Meteorological data including
84 relative humidity (RH) and air temperature (T) were measured by an automatic weather station (model MetPak, Gill
85 Instruments Limited, UK). Time used in the present study is local time (LT = UTC + 8).

86 **2.2 Measurements of ions and isotopic ratios**

87 Ion concentrations of NO_3^- and Cl^- were measured in Anhui Province Key Laboratory of Polar Environment and Global
88 Change in the University of Science and Technology of China. A detailed description of this method can be found in the

89 literature (Ye et al., 2015). Briefly, ions in the PM_{2.5} filter sample were extracted with Millipore water ($\geq 18 \text{ M}\Omega$) and
 90 insoluble substances in the extract were filtered. Then the ion concentrations were analyzed by an ion chromatograph system
 91 (model Dionex ICS-2100, Thermo Fisher Scientific Inc., USA). The measured ion concentrations of blank samples were
 92 subtracted when determining the ion concentrations of real samples. Typical analytical precision by our method is better than
 93 10 % relative standard deviation (RSD) (Chen et al., 2016).

94 $\delta^{15}\text{N}(\text{NO}_3^-)$ and $\Delta^{17}\text{O}(\text{NO}_3^-)$ were measured with a bacterial denitrifier method (Kaiser et al., 2007) in IsoLab at the
 95 University of Washington, USA. Briefly, ions in the filter sample were extracted with Millipore water ($\geq 18 \text{ M}\Omega$) and the
 96 insoluble substances were filtered. NO_3^- in each sample was converted to N_2O by the denitrifying bacteria, *Pseudomonas*
 97 *aureofaciens*. Then N_2 and O_2 , which were decomposed from N_2O in a gold tube at 800°C , were separated by a gas
 98 chromatograph. The isotopic ratios of each gas were then measured by a Finnigan Delta-Plus Advantage isotope ratio mass
 99 spectrometer. Masses of 28 and 29 from N_2 were measured to determine $\delta^{15}\text{N}$. Masses of 32, 33 and 34 from O_2 were
 100 measured to determine $\delta^{17}\text{O}$ and $\delta^{18}\text{O}$ and $\Delta^{17}\text{O}$ was then calculated. We use international nitrate reference materials,
 101 USGS34, USGS35 and IAEANO₃, for data calibration. The uncertainty (1σ) of $\delta^{15}\text{N}$ and $\Delta^{17}\text{O}$ measurements in our method
 102 is 0.4 ‰ and 0.2 ‰, respectively, based on replicate analysis of the international reference materials. All the samples
 103 including blank samples were measured in triplicate to quantify the uncertainty in each sample. The blank was subtracted for
 104 each sample by using an isotopic mass balance on the basis of isotopic ratios and concentrations of the blank. To minimize
 105 the blank effect, samples with blank concentrations being $> 10\%$ of their concentrations were not analyzed for isotopic
 106 ratios. This ruled out 3 of the total 34 samples, all of which are in non-polluted days (NPD, $\text{PM}_{2.5} < 75 \mu\text{g m}^{-3}$). Totally,
 107 isotopic compositions of 7 samples in NPD and 24 samples in polluted days (PD, $\text{PM}_{2.5} \geq 75 \mu\text{g m}^{-3}$) are reported here.

108 2.3 Estimate of different nitrate formation pathways based on $\Delta^{17}\text{O}(\text{NO}_3^-)$

109 The observed $\Delta^{17}\text{O}(\text{NO}_3^-)$ is determined by the relative importance of different nitrate formation pathways and the
 110 relative importance of O_3 oxidation in NO_x cycling as shown in Eq. (1):

$$111 \Delta^{17}\text{O}(\text{NO}_3^-) = \Delta^{17}\text{O}_{\text{R6}} \times f_{\text{R6}} + \Delta^{17}\text{O}_{\text{R7}} \times f_{\text{R7}} + \Delta^{17}\text{O}_{\text{R8}} \times f_{\text{R8}} + \Delta^{17}\text{O}_{\text{R9}} \times f_{\text{R9}} + \Delta^{17}\text{O}_{\text{R10}} \times f_{\text{R10}} \quad (1)$$

112 Where $\Delta^{17}\text{O}_{\text{R6}}$, $\Delta^{17}\text{O}_{\text{R7}}$, $\Delta^{17}\text{O}_{\text{R8}}$, $\Delta^{17}\text{O}_{\text{R9}}$ and $\Delta^{17}\text{O}_{\text{R10}}$ is respectively $\Delta^{17}\text{O}(\text{NO}_3^-)$ resulting from $\text{NO}_2 + \text{OH}$, $\text{NO}_2 + \text{H}_2\text{O}$, $\text{NO}_3 +$
 113 HC , $\text{N}_2\text{O}_5 + \text{H}_2\text{O}$ and $\text{N}_2\text{O}_5 + \text{Cl}^-$ pathway (Table 1). f_{R6} , f_{R7} , f_{R8} , f_{R9} and f_{R10} is respectively corresponding fractional
 114 contribution of above pathways to nitrate production. By using the $\Delta^{17}\text{O}$ assumptions for different pathways in Table 1 and
 115 the definition $f_{\text{R6}} + f_{\text{R7}} + f_{\text{R8}} + f_{\text{R9}} + f_{\text{R10}} = 1$, Eq. (1) is further expressed as:

$$116 \Delta^{17}\text{O}(\text{NO}_3^-)/\text{‰} = 25\alpha f_{\text{R6}} + 25\alpha f_{\text{R7}} + (25\alpha + 14) \times f_{\text{R8}} + (25\alpha + 7) \times f_{\text{R9}} + (25\alpha + 14) \times f_{\text{R10}} = 25\alpha + 14 \times$$

$$117 (f_{\text{R8}} + f_{\text{R10}}) + 7f_{\text{R9}} \quad (2)$$

118 Where α is the proportion of O_3 oxidation in NO_2 production rate, calculated by Eq. (3):

$$\alpha = \frac{k_{R1}[\text{NO}][\text{O}_3]}{k_{R1}[\text{NO}][\text{O}_3] + k_{R2a}[\text{NO}][\text{HO}_2] + k_{R2b}[\text{NO}][\text{RO}_2]} \quad (3)$$

In Eq. (3), k_{R1} , k_{R2a} and k_{R2b} is respectively the reaction rate constant listed in Table 2. To evaluate α , we estimated HO_2 mixing ratios on the basis of empirical formulas between HO_2 and O_3 mixing ratios derived from observations in winter (Kanaya et al., 2007), that's: $[\text{HO}_2]/(\text{pmol mol}^{-1}) = \exp(5.7747 \times 10^{-2} \times [\text{O}_3]/(\text{nmol mol}^{-1}) - 1.7227)$ during the day time and $[\text{HO}_2]/(\text{pmol mol}^{-1}) = \exp(7.7234 \times 10^{-2} \times [\text{O}_3]/(\text{nmol mol}^{-1}) - 1.6363)$ at night. Then RO_2 mixing ratio was calculated as 70 % of HO_2 mixing ratios based on previous studies (Liu et al., 2012; Elshorbany et al., 2012; Mihelcic et al., 2003). As NO mixing ratio was not observed in our study, we estimated NO mixing ratios following the empirical formulas between NO_x and CO mixing ratios derived from observations in winter Beijing (Lin et al., 2011), that's: $[\text{NO}]/(\text{nmol mol}^{-1}) = ([\text{CO}]/(\text{nmol mol}^{-1}) - 196)/27.3 - [\text{NO}_2]/(\text{nmol mol}^{-1})$ during daytime and $[\text{NO}]/(\text{nmol mol}^{-1}) = ([\text{CO}]/(\text{nmol mol}^{-1}) - 105)/30.9 - [\text{NO}_2]/(\text{nmol mol}^{-1})$ at night.

By using Eq. (2), the relative importance of nocturnal formation pathways ($f_{R8} + f_{R9} + f_{R10}$) can be written as Eq. (4):

$$f_{R8} + f_{R9} + f_{R10} = \frac{f_{R9}}{2} + \frac{\Delta^{17}\text{O}(\text{NO}_3^-)}{14\text{‰}} - 1.8\alpha \quad (4)$$

Eq. (4) suggests that the relative importance of nocturnal pathways is solely a function of the assumption of f_{R9} at given $\Delta^{17}\text{O}(\text{NO}_3^-)$ and α . Since f_{R9} , $f_{R8} + f_{R10}$ and $f_{R8} + f_{R9} + f_{R10}$ should be in the range of 0 – 1 all the time, f_{R9} is further limited to meet Eq. (5):

$$f_{R9} \begin{cases} > 0 \\ < \min(1, \frac{\Delta^{17}\text{O}(\text{NO}_3^-)}{7\text{‰}} - 3.6\alpha, 2 + 3.6\alpha - \frac{\Delta^{17}\text{O}(\text{NO}_3^-)}{7\text{‰}}) \end{cases} \quad (5)$$

We estimated the relative importance of nocturnal pathways ($f_{R8} + f_{R9} + f_{R10}$) by using concentration-weighted $\Delta^{17}\text{O}(\text{NO}_3^-)$ observations and production rate weighted α in PD of each haze event rather than each sample due to the lifetime of atmospheric nitrate is typically on the order of day (Liang et al., 1998), larger than our sampling collection interval.

2.4 Simulation of surface N_2O_5 and NO_3 radical

To see whether the relative importance of nocturnal pathways constrained by $\Delta^{17}\text{O}(\text{NO}_3^-)$ can be reproduced by models, we use the standard Master Chemical Mechanism (MCM, version 3.3, <http://mcm.leeds.ac.uk/>) to simulate the mixing ratios of surface N_2O_5 and NO_3 radical during our sampling period. The input for this modeling work includes: (i) 1 h-averaged mixing ratios of observed surface CO , NO_2 , SO_2 and O_3 and estimated NO (see Sect. 2.3), (ii) observed RH and T , and (iii) the mixing ratios of organic compounds from the literatures (Table S1) (Wang et al., 2001; Wu et al., 2016; Rao et al., 2016).

147 3.1 Overview of observations in Beijing haze

148 Figure 3 describes general characteristics of haze events during our observations. The 12h-averaged $PM_{2.5}$
 149 concentrations, corresponding with filter samples, varied from 16 to 323 $\mu g m^{-3}$ with a mean of $(141 \pm 88 (1SD)) \mu g m^{-3}$. In
 150 comparison, the Grade II of NAAQS (National Ambient Air Quality Standard) in China is 75 $\mu g m^{-3}$ for daily $PM_{2.5}$. The
 151 NO_3^- concentrations present similar trends with $PM_{2.5}$ levels (Fig. 3a), ranged from 0.3 to 106.7 $\mu g m^{-3}$ with a mean of
 152 $(6.1 \pm 5.3) \mu g m^{-3}$ in non-polluted days (NPD, $PM_{2.5} < 75 \mu g m^{-3}$) and $(48.4 \pm 24.7) \mu g m^{-3}$ in polluted days (PD, $PM_{2.5} \geq 75 \mu g$
 153 m^{-3}). Correspondingly, the nitrogen oxidation ratio (NOR, which equals to NO_3^- molar concentration divided by the sum of
 154 NO_3^- and NO_2 molar concentration), a proxy for secondary transformation of nitrate (Sun et al., 2006), increased from a
 155 mean of 0.09 ± 0.05 in NPD to 0.31 ± 0.10 in PD (Fig. 3b). In residential heating season (Case III – V in November 2014 –
 156 January 2015, Fig. 3b), Cl^- concentrations present similar trends with NO_3^- levels, increased from $(0.6 \pm 1.0) \mu g m^{-3}$ in NPD
 157 to $(7.9 \pm 4.8) \mu g m^{-3}$ in PD. However, during Case I – II in October 2014, Cl^- concentrations were $(3.5 \pm 1.6) \mu g m^{-3}$ in NPD
 158 and $(3.5 \pm 1.9) \mu g m^{-3}$ in PD, showing no significant difference at 0.01 level (t-test). Throughout our observational period, the
 159 visibility decreased from $(11.4 \pm 6.7) km$ in NPD to $(3.1 \pm 1.8) km$ in PD (Fig. 3c) while relative humidity (RH) increased from
 160 $(37 \pm 12) \%$ in NPD to $(62 \pm 12) \%$ in PD (Fig. 3d).

161 $\Delta^{17}O(NO_3^-)$ ranged from 27.5 ‰ to 33.9 ‰ with the mean of $(29.1 \pm 1.3) \%$ in NPD and $(31.0 \pm 1.7) \%$ in PD (Fig. 3c).
 162 Our observed $\Delta^{17}O(NO_3^-)$ is in the range of aerosol $\Delta^{17}O(NO_3^-)$ reported in literatures (Table 3) and similar to wet deposition
 163 $\Delta^{17}O(NO_3^-)$ observed in East Asia (Nelson et al., 2018; Tsunogai et al., 2016; Tsunogai et al., 2010). All our observed
 164 $\Delta^{17}O(NO_3^-)$ values, no matter daytime sample (08:00 – 20:00) or nighttime sample (20:00 – 08:00), are larger than 25 ‰, the
 165 maximum of $\Delta^{17}O(NO_3^-)$ that can be produced via $NO_2 + OH$ and $NO_2 + H_2O$ (Table 1) at the assumption of bulk $\Delta^{17}O(O_3)$
 166 = 26 ‰ (Ishino et al., 2017; Vicars and Savarino, 2014). This directly suggests nocturnal formation pathways ($N_2O_5 +$
 167 H_2O/Cl^- and $NO_3 + HC$) must contribute to all the sampled nitrate. Given the lifetime of atmospheric nitrate is typically
 168 larger than our sampling collection interval (Vicars et al., 2013), each of our samples is expected to reflect both daytime and
 169 nocturnal nitrate production. Not surprisingly, $\Delta^{17}O(NO_3^-)$ mean of daytime and nighttime samples is $(30.3 \pm 1.5) \%$ and
 170 $(30.9 \pm 2.1) \%$, respectively, showing no significant difference at 0.01 level (t-test).

171 $\delta^{15}N(NO_3^-)$ in our observation varied from -2.5 ‰ to 19.2 ‰ with a mean of $(7.4 \pm 6.8) \%$, which is in the range of
 172 $\delta^{15}N(NO_3^-)$ observed from rainwater in Beijing, China (Zhang et al., 2008) and similar to $\delta^{15}N(NO_3^-)$ values observed from
 173 aerosols in Germany (Freyer, 1991). Figure 3d shows that $\delta^{15}N(NO_3^-)$ varies largely in October 2014. The mean $\delta^{15}N(NO_3^-)$
 174 varied from $(0.4 \pm 1.5) \%$ in 08:00 Oct. 18 – 08:00 Oct. 21 to $(10.7 \pm 1.4) \%$ in 08:00 Oct. 21 – 08:00 Oct. 23 and then
 175 decreased to $(-0.9 \pm 2.1) \%$ in 08:00 Oct. 23 – 08:00 Oct. 26, which corresponds to $PM_{2.5}$ concentrations being 155 ± 63 ,

176 57 ± 19 and $(188 \pm 51) \mu\text{g m}^{-3}$ respectively. However, during residential heating season, relatively high $\delta^{15}\text{N}(\text{NO}_3^-)$ (7.6 –
177 19.2 ‰) were always observed both in NPD and PD. This may be related to the high NO_x emission from coal combustion in
178 north China (Wang et al., 2012; Lin, 2012; Zhang et al., 2007).

179 3.2 Relationships between $\Delta^{17}\text{O}(\text{NO}_3^-)$ and other data

180 Figure 4 presents the relationships between $\Delta^{17}\text{O}(\text{NO}_3^-)$ and NO_3^- concentrations, $\text{PM}_{2.5}$ concentrations, NOR, visibility,
181 RH and $\delta^{15}\text{N}(\text{NO}_3^-)$. $\Delta^{17}\text{O}(\text{NO}_3^-)$ shows a positive correlation with NO_3^- concentrations when $\text{NO}_3^- < 50 \mu\text{g m}^{-3}$ ($r = 0.81$, p
182 < 0.01). Similarly, $\Delta^{17}\text{O}(\text{NO}_3^-)$ shows a positive correlation with $\text{PM}_{2.5}$ concentration in Fig. 4b and NOR in Fig. 4c when
183 $\text{NO}_3^- < 50 \mu\text{g m}^{-3}$ ($r = 0.71$ and $r = 0.80$, $p < 0.01$, respectively). Figure 4d shows that $\Delta^{17}\text{O}(\text{NO}_3^-)$ is negative correlated with
184 visibility in general ($r = -0.66$, $p < 0.01$). The significant decrease of visibility will largely reduce surface radiation and
185 thereby OH mixing ratios (Zheng et al., 2015b), which is unfavorable for nitrate production via $\text{NO}_2 + \text{OH}$ pathway. Since
186 $\text{NO}_2 + \text{OH}$ pathway produces low $\Delta^{17}\text{O}(\text{NO}_3^-)$ (Table 1), the decreased importance of $\text{NO}_2 + \text{OH}$ pathway will conversely
187 increase $\Delta^{17}\text{O}(\text{NO}_3^-)$. While the raise of RH accompanying the large increase of $\text{PM}_{2.5}$ favors nitrate production via
188 heterogeneous uptake of gases, e.g., N_2O_5 (Zheng et al., 2015b; Zheng et al., 2015a) and heterogeneous uptake of N_2O_5
189 produces relative high $\Delta^{17}\text{O}(\text{NO}_3^-)$ (Table 1), the enhanced heterogeneous uptake of N_2O_5 will increase $\Delta^{17}\text{O}(\text{NO}_3^-)$ too.
190 Therefore, the decrease of importance of $\text{NO}_2 + \text{OH}$ and the increase of importance of heterogeneous uptake of N_2O_5 should
191 be responsible for the positive correlation between $\Delta^{17}\text{O}(\text{NO}_3^-)$ and NO_3^- concentrations. In addition, for samples with $\text{NO}_3^- >$
192 $50 \mu\text{g m}^{-3}$, visibility was always low with narrow variations (2.3 ± 1.0 km) and RH was always high with narrow range
193 (67 ± 7 %), which may be responsible for the relatively high $\Delta^{17}\text{O}(\text{NO}_3^-)$ being observed (31.2 ± 1.7 ‰). Figure 4f shows that
194 $\Delta^{17}\text{O}(\text{NO}_3^-)$ is not correlated with $\delta^{15}\text{N}(\text{NO}_3^-)$.

195 3.3 Estimate of nocturnal formation pathways

196 Before estimating the relative importance of different nitrate formation pathways, we estimate the proportion of O_3
197 oxidation in NO_2 production rate, α . The possible α range can be calculated based on observed $\Delta^{17}\text{O}(\text{NO}_3^-)$. It can be
198 obtained from Table 1 that $25\alpha \text{ ‰} < \Delta^{17}\text{O}(\text{NO}_3^-) < (25\alpha + 14) \text{ ‰}$, so the lower limit of possible α is $(\Delta^{17}\text{O}(\text{NO}_3^-) -$
199 $14 \text{ ‰})/25 \text{ ‰}$. And since $\Delta^{17}\text{O}(\text{NO}_3^-) \geq 27.5 \text{ ‰}$ in our observation, the higher limit of α is always 1 for all the samples. Figure
200 5 presents the possible range of calculated α based on $\Delta^{17}\text{O}(\text{NO}_3^-)$. The calculated lower limit of α ranged from 0.56 to 0.81
201 with a mean of 0.68 ± 0.07 , which directly suggests that O_3 oxidation played a dominated role in NO_x cycling during Beijing
202 haze. To estimate the specific α value, chemical kinetics in Table 2 and Eq. (3) were used. Specific α is estimated to range
203 from 0.86 to 0.97 with a mean of (0.94 ± 0.03) , which is in the possible range of α value calculated directly based on
204 $\Delta^{17}\text{O}(\text{NO}_3^-)$ (Fig. 5) and close to the range of 0.85 – 1 determined in other mid-latitude areas (Michalski et al., 2003; Patris et

205 al., 2007).

206 Figure 6a shows the estimated relative importance of nocturnal formation pathways ($\text{N}_2\text{O}_5 + \text{H}_2\text{O}/\text{Cl}^-$ and $\text{NO}_3 + \text{HC}$)
207 during PD of each case on the basis of observed $\Delta^{17}\text{O}(\text{NO}_3^-)$. Possible fractional contribution of nocturnal formation
208 pathways ranges from 49 – 97 %, 58 – 100 %, 60 – 100 %, 45 – 90 % and 70 – 100 % in PD of Case I to V, respectively,
209 with a mean of 56 – 97 %. This directly implies that nocturnal chemistry dominates atmospheric nitrate production in Beijing
210 haze. This finding is consistent with the suggested importance of heterogeneous uptake of N_2O_5 during Beijing haze by
211 previous studies (Su et al., 2017; Wang et al., 2017b). The other pathways ($\text{NO}_2 + \text{OH}$ and $\text{NO}_2 + \text{H}_2\text{O}$) account for the
212 remaining fraction with a mean possible range of 3 – 44 %. Since $\text{NO}_2 + \text{OH}$ and $\text{NO}_2 + \text{H}_2\text{O}$ produces the same $\Delta^{17}\text{O}(\text{NO}_3^-)$
213 signature in our assumptions (Table 1), we cannot distinguish their fractional contribution barely from the observed
214 $\Delta^{17}\text{O}(\text{NO}_3^-)$ in the present study. However, the overall positive correlation between $\Delta^{17}\text{O}(\text{NO}_3^-)$ and RH ($r = 0.55$, $p < 0.01$,
215 Fig. 4e) suggests heterogeneous uptake of NO_2 should be less important than heterogeneous uptake of N_2O_5 , otherwise, a
216 negative relationship between $\Delta^{17}\text{O}(\text{NO}_3^-)$ and RH is expected. Our calculations also suggest that the sum of possible
217 fractional contribution of $\text{N}_2\text{O}_5 + \text{Cl}^-$ and $\text{NO}_3 + \text{HC}$ is in the range of 0 – 49 %, 17 – 58 %, 20 – 60 %, 0 – 45 % and 41 – 70 %
218 in PD of Case I to V, respectively, with a mean of 16 – 56 % (Table 4), which emphasizes that $\text{N}_2\text{O}_5 + \text{Cl}^-$ and $\text{NO}_3 + \text{HC}$
219 played a non-ignorable role in nitrate production during Beijing haze. Due to that $\text{N}_2\text{O}_5 + \text{Cl}^-$ and $\text{NO}_3 + \text{HC}$ produce the
220 same $\Delta^{17}\text{O}(\text{NO}_3^-)$ in our assumptions (Table 1), we cannot distinguish their fractional contribution barely from the observed
221 $\Delta^{17}\text{O}(\text{NO}_3^-)$ in this study, either. However, $\text{NO}_3 + \text{HC}$ should be minor for nitrate production. For example, 3D modelling
222 work of Alexander et al. (2009) suggests $\text{NO}_3 + \text{HC}$ pathway only accounts for 4 % of global tropospheric nitrate production
223 annually on average, and Michalski et al. (2003) found that $\text{NO}_3 + \text{HC}$ pathway contributes 1 – 10 % to nitrate production on
224 the basis of an annual observation at La Jolla, California, with low values in winter. Therefore, in addition to $\text{NO}_3 + \text{HC}$,
225 $\text{N}_2\text{O}_5 + \text{Cl}^-$ is likely to also contribute to nitrate production during haze in Beijing. Supportively, the concentrations of Cl^- is
226 as high as $(5.5 \pm 4.1) \mu\text{g m}^{-3}$ during PD of all the cases in our observation and the mixing ratios of ClNO_2 , an indicator of
227 $\text{N}_2\text{O}_5 + \text{Cl}^-$ pathway, reached up to $2.9 \text{ nmol mol}^{-1}$ during a summer observation in suburban Beijing (Wang et al., 2018b)
228 and reached up to $5.0 \text{ nmol mol}^{-1}$ in a modelling work in summer rural Beijing (Wang et al., 2017c).

229 Figure 6b presents the simulated mixing ratios of surface N_2O_5 and NO_3 radical during our observational period by
230 using the box model MCM. The 12h averaged mixing ratios of simulated N_2O_5 ranged from 3 to $649 \text{ pmol mol}^{-1}$ while
231 simulated NO_3 radical ranged from 0 to 27 pmol mol^{-1} . In comparison, previous observations in Beijing suggest 5s averaged
232 N_2O_5 can be as high as $1.3 \text{ nmol mol}^{-1}$ and 30 min averaged NO_3 radical can be as high as 38 pmol mol^{-1} with large
233 day-to-day variability (Wang et al., 2017b; Wang et al., 2015). During Case I and II in October, simulated N_2O_5 and NO_3
234 radical present similar trends with the observed NO_3^- and remain relatively high during PD ($346 \pm 128 \text{ pmol mol}^{-1}$ and 9 ± 7
235 pmol mol^{-1} , respectively, Fig. 6b), which supports the dominant role of nocturnal formation pathways suggested by
236 $\Delta^{17}\text{O}(\text{NO}_3^-)$. However, during Case III – V in residential heating season, the simulated surface mixing ratios of N_2O_5 and

237 NO₃ radical remain relatively low during PD (63 ± 80 pmol mol⁻¹ and < 1 pmol mol⁻¹, respectively, Fig. 6b), which seems to
238 be inconsistent with $\Delta^{17}\text{O}(\text{NO}_3^-)$ observations. We note that a recent study suggests that heterogeneous uptake of N₂O₅ is
239 negligible at surface but larger at higher altitudes (e.g., > 150 m) during winter haze in Beijing (Wang et al., 2018a). So
240 during PD of Case III – V in our observational period, large nitrate production via heterogeneous uptake of N₂O₅ may occur
241 aloft rather than at surface, which leads to the dominant role of nocturnal formation pathways as suggested by $\Delta^{17}\text{O}(\text{NO}_3^-)$.

242 4 Conclusions

243 We report the first observation of isotopic composition ($\Delta^{17}\text{O}$ and $\delta^{15}\text{N}$) of atmospheric nitrate in Beijing haze. The
244 observed $\Delta^{17}\text{O}(\text{NO}_3^-)$ ranged from 27.5 ‰ to 33.9 ‰ with a mean of (30.6 ± 1.8) ‰. $\delta^{15}\text{N}(\text{NO}_3^-)$ ranged largely from -2.5 ‰
245 to 19.2 ‰ with a mean of (7.4 ± 6.8) ‰. When NO₃⁻ is < 50 μg m⁻³, a positive correlation was observed between $\Delta^{17}\text{O}(\text{NO}_3^-)$
246 and NO₃⁻ concentration ($r = 0.81$, $p < 0.01$). This is likely to result from the variation of relative importance of different
247 nitrate formation pathway. Calculations with the constraint of $\Delta^{17}\text{O}(\text{NO}_3^-)$ suggest that nocturnal pathways (N₂O₅ + H₂O/Cl⁻
248 and NO₃ + HC) dominated nitrate production during polluted days ($\text{PM}_{2.5} \geq 75$ μg m⁻³), with the mean possible contribution
249 of 56 – 97 %. $\Delta^{17}\text{O}(\text{NO}_3^-)$ also indicates that O₃ dominated NO oxidation during Beijing haze.

250 Supplementary Materials

251 **Figure S1.** The diurnal differences of observed NO₂, CO and O₃ and calculated NO, HO₂ and RO₂ during our sampling
252 periods.

253 **Table S1.** The input of organic compounds for MCM model (nmol mol⁻¹).

254 Data availability

255 All data needed to draw the conclusions are present in the main text and/or the Supplementary Materials. For additional
256 data, please contact the corresponding author (zqxie@ustc.edu.cn).

257 Author contributions

258 Z.Q.X. conceived this study. P.Z.H. conducted isotope measurements. P.Z.H., X.Y.C, S.D.F., H.C.Z., H. K. performed
259 the field experiments and ion measurements. P.Z.H., Z.Q.X., X.W.Y. interpreted the data. C.L. contributed to the field
260 observation support. P.Z.H. wrote the manuscript with Z.Q.X. inputs. All authors involved the discussion and revision.

261 **Competing interests**

262 The authors declare no competing interests.

263 **Acknowledgments**

264 This work was supported by the National Key Project of MOST (2016YFC0203302), NSFC (91544013), the Key
265 Project of CAS (KJZD-EW-TZ-G06-01) and the Atmospheric Pollution Control of the Prime Minister (DQGG0104). We
266 gratefully thank staffs of IsoLab at UW for their technical support, Becky Alexander and Lei Geng for helpful discussions.

267 **References**

- 268 Alexander, B., Hastings, M. G., Allman, D. J., Dachs, J., Thornton, J. A., and Kunasek, S. A.: Quantifying atmospheric
269 nitrate formation pathways based on a global model of the oxygen isotopic composition ($\Delta^{17}\text{O}$) of atmospheric nitrate,
270 *Atmos. Chem. Phys.*, 9, 5043-5056, 2009.
- 271 Berhanu, T. A., Savarino, J., Bhattacharya, S. K., and Vicars, W. C.: ^{17}O excess transfer during the $\text{NO}_2 + \text{O}_3 \rightarrow \text{NO}_3 + \text{O}_2$
272 reaction, *J. Chem. Phys.*, 136, 044311, 2012.
- 273 Bertram, T. H., and Thornton, J. A.: Toward a general parameterization of N_2O_5 reactivity on aqueous particles: the
274 competing effects of particle liquid water, nitrate and chloride, *Atmos. Chem. Phys.*, 9, 8351-8363, 2009.
- 275 Beyn, F., Matthias, V., and Dänke, K.: Changes in atmospheric nitrate deposition in Germany—An isotopic perspective,
276 *Environ. Pollut.*, 194, 1-10, 2014.
- 277 Brenninkmeijer, C. A., Janssen, C., Kaiser, J., Röckmann, T., Rhee, T. S., and Assonov, S. S.: Isotope effects in the chemistry
278 of atmospheric trace compounds, *Chem. Rev.*, 103, 5125-5162, 2003.
- 279 Brook, R. D., Rajagopalan, S., Pope, C. A., Brook, J. R., Bhatnagar, A., Diez-Roux, A. V., Holguin, F., Hong, Y., Luepker, R.
280 V., and Mittleman, M. A.: Particulate matter air pollution and cardiovascular disease an update to the scientific
281 statement from the American Heart Association, *Circulation*, 121, 2331-2378, 2010.
- 282 Brown, S. S., and Stutz, J.: Nighttime radical observations and chemistry, *Chem. Soc. Rev.*, 41, 6405-6447, 2012.
- 283 Burkholder, J. B., Sander, S. P., Abbatt, J. P. D., Barker, J. R., Huie, R. E., Kolb, C. E., Kurylo, M. J., Orkin, V. L., Wilmouth,
284 D. M., and Wine, P. H.: *Chemical Kinetics and Photochemical Data for Use in Atmospheric Studies: Evaluation*
285 *Number 18*, Pasadena, CA: Jet Propulsion Laboratory, National Aeronautics and Space Administration, 2015.
- 286 Chen, Q., Geng, L., Schmidt, J. A., Xie, Z., Kang, H., Dachs, J., Cole-Dai, J., Schauer, A. J., Camp, M. G., and Alexander, B.:

287 Isotopic constraints on the role of hypohalous acids in sulfate aerosol formation in the remote marine boundary layer,
288 *Atmos. Chem. Phys.*, 16, 11433-11450, 2016.

289 Chen, Z., Zhang, J., Zhang, T., Liu, W., and Liu, J.: Haze observations by simultaneous lidar and WPS in Beijing before and
290 during APEC, 2014, *Sci. China Chem.*, 58, 1385-1392, 2015.

291 Cheng, Z., Jiang, J., Fajardo, O., Wang, S., and Hao, J.: Characteristics and health impacts of particulate matter pollution in
292 China (2001–2011), *Atmos. Environ.*, 65, 186-194, 2013.

293 Cheung, J. L., Li, Y., Boniface, J., Shi, Q., Davidovits, P., Worsnop, D. R., Jayne, J. T., and Kolb, C. E.: Heterogeneous
294 interactions of NO₂ with aqueous surfaces, *J. Phys. Chem. A*, 104, 2655-2662, 2000.

295 Elliott, E. M., Kendall, C., Boyer, E. W., Burns, D. A., Lear, G. G., Golden, H. E., Harlin, K., Bytnerowicz, A., Butler, T. J.,
296 and Glatz, R.: Dual nitrate isotopes in dry deposition: Utility for partitioning NO_x source contributions to landscape
297 nitrogen deposition, *J. Geophys. Res. Biogeo.*, 114, 2009.

298 Elshorbany, Y. F., Kleffmann, J., Hofzumahaus, A., Kurtenbach, R., Wiesen, P., Brauers, T., Bohn, B., Dorn, H. P., Fuchs, H.,
299 and Holland, F.: HO_x budgets during HO_xComp: A case study of HO_x chemistry under NO_x - limited conditions, *J.*
300 *Geophys. Res.*, 117, 2012.

301 Fang, Y., Koba, K., Wang, X., Wen, D., Li, J., Takebayashi, Y., Liu, X., and Yoh, M.: Anthropogenic imprints on nitrogen and
302 oxygen isotopic composition of precipitation nitrate in a nitrogen-polluted city in southern China, *Atmos. Chem. Phys.*,
303 11, 1313-1325, 2011.

304 Felix, J. D., Elliott, E. M., and Shaw, S. L.: Nitrogen isotopic composition of coal-fired power plant NO_x: influence of
305 emission controls and implications for global emission inventories, *Environ. Sci. Technol.*, 46, 3528-3535, 2012.

306 Freyer, H. D.: Seasonal variation of ¹⁵N/¹⁴N ratios in atmospheric nitrate species, *Tellus B*, 43, 30-44, 1991.

307 Freyer, H. D., Kley, D., Volz - Thomas, A., and Kobel, K.: On the interaction of isotopic exchange processes with
308 photochemical reactions in atmospheric oxides of nitrogen, *J. Geophys. Res. Atmos.*, 98, 14791-14796, 1993.

309 Geng, L., Alexander, B., Cole-Dai, J., Steig, E. J., Savarino, J., Sofen, E. D., and Schauer, A. J.: Nitrogen isotopes in ice core
310 nitrate linked to anthropogenic atmospheric acidity change, *Proc. Natl. Acad. Sci. USA*, 111, 5808-5812, 2014.

311 Goodman, A. L., Underwood, G. M., and Grassian, V. H.: Heterogeneous reaction of NO₂: Characterization of gas-phase and
312 adsorbed products from the reaction, 2NO₂(g) + H₂O(a) → HONO(g) + HNO₃(a) on hydrated silica particles, *J. Phys.*
313 *Chem. A*, 103, 7217-7223, 1999.

314 Guha, T., Lin, C. T., Bhattacharya, S. K., Mahajan, A. S., Ou-Yang, C.-F., Lan, Y.-P., Hsu, S. C., and Liang, M.-C.: Isotopic
315 ratios of nitrate in aerosol samples from Mt. Lulin, a high-altitude station in Central Taiwan, *Atmos. Environ.*, 154,
316 53-69, 2017.

317 Hastings, M. G., Casciotti, K. L., and Elliott, E. M.: Stable isotopes as tracers of anthropogenic nitrogen sources, deposition,
318 and impacts, *Elements*, 9, 339-344, 2013.

319 He, P., Alexander, B., Geng, L., Chi, X., Fan, S., Zhan, H., Kang, H., Zheng, G., Cheng, Y., Su, H., Liu, C., and Xie, Z.:
320 Isotopic constraints on heterogeneous sulfate production in Beijing haze, *Atmos. Chem. Phys.*, 18, 5515-5528, 2018.

321 Hoering, T.: The isotopic composition of the ammonia and the nitrate ion in rain, *Geochim. Cosmochim. Acta*, 12, 97-102,
322 1957.

323 Ishino, S., Hattori, S., Savarino, J., Jourdain, B., Preunkert, S., Legrand, M., Caillon, N., Barbero, A., Kuribayashi, K., and
324 Yoshida, N.: Seasonal variations of triple oxygen isotopic compositions of atmospheric sulfate, nitrate, and ozone at
325 Dumont d'Urville, coastal Antarctica, *Atmos. Chem. Phys.*, 17, 3713-3727, 2017.

326 Kaiser, J., Hastings, M. G., Houlton, B. Z., Röckmann, T., and Sigman, D. M.: Triple oxygen isotope analysis of nitrate using
327 the denitrifier method and thermal decomposition of N₂O, *Anal. Chem.*, 79, 599-607, 2007.

328 Kanaya, Y., Cao, R., Akimoto, H., Fukuda, M., Komazaki, Y., Yokouchi, Y., Koike, M., Tanimoto, H., Takegawa, N., and
329 Kondo, Y.: Urban photochemistry in central Tokyo: 1. Observed and modeled OH and HO₂ radical concentrations
330 during the winter and summer of 2004, *J. Geophys. Res.*, 112, 2007.

331 Kunasek, S. A., Alexander, B., Steig, E. J., Hastings, M. G., Gleason, D. J., and Jarvis, J. C.: Measurements and modeling of
332 $\Delta^{17}\text{O}$ of nitrate in snowpits from Summit, Greenland, *J. Geophys. Res.*, 113, 2008.

333 Li, H., Zhu, T., Zhao, D., Zhang, Z., and Chen, Z.: Kinetics and mechanisms of heterogeneous reaction of NO₂ on CaCO₃
334 surfaces under dry and wet conditions, *Atmos. Chem. Phys.*, 10, 463-474, 2010.

335 Li, Z., Hu, R., Xie, P., Wang, H., Lu, K., and Wang, D.: Intercomparison of in situ CRDS and CEAS for measurements of
336 atmospheric N₂O₅ in Beijing, China, *Sci. Total Environ.*, 613, 131-139, 2018.

337 Liang, J., Horowitz, L. W., Jacob, D. J., Wang, Y., Fiore, A. M., Logan, J. A., Gardner, G. M., and Munger, J. W.: Seasonal
338 budgets of reactive nitrogen species and ozone over the United States, and export fluxes to the global atmosphere, *J.*
339 *Geophys. Res. Atmos.*, 103, 13435-13450, 1998.

340 Lin, J.-T.: Satellite constraint for emissions of nitrogen oxides from anthropogenic, lightning and soil sources over East
341 China on a high-resolution grid, *Atmos. Chem. Phys.*, 12, 2881-2898, 2012.

342 Lin, W., Xu, X., Ge, B., and Liu, X.: Gaseous pollutants in Beijing urban area during the heating period 2007–2008:
343 variability, sources, meteorological, and chemical impacts, *Atmos. Chem. Phys.*, 11, 8157-8170, 2011.

344 Liu, Z., Wang, Y., Gu, D., Zhao, C., Huey, L., Stickel, R., Liao, J., Shao, M., Zhu, T., and Zeng, L.: Summertime
345 photochemistry during CAREBeijing-2007: ROx budgets and O₃ formation, *Atmos. Chem. Phys.*, 12, 7737-7752, 2012.

346 Michalski, G., Scott, Z., Kabling, M., and Thiemens, M. H.: First measurements and modeling of $\Delta^{17}\text{O}$ in atmospheric
347 nitrate, *Geophys. Res. Lett.*, 30, 2003.

348 Mihelcic, D., Holland, F., Hofzumahaus, A., Hoppe, L., Konrad, S., Müssen, P., Pätz, H. W., Schäfer, H. J., Schmitz, T., and
349 Volz - Thomas, A.: Peroxy radicals during BERLIOZ at Pabstthum: Measurements, radical budgets and ozone
350 production, *J. Geophys. Res.*, 108, 2003.

351 Morin, S., Savarino, J., Bekki, S., Cavender, A., Shepson, P. B., and Bottenheim, J. W.: Major influence of BrO on the NO_x
352 and nitrate budgets in the Arctic spring, inferred from $\Delta^{17}\text{O}(\text{NO}_3^-)$ measurements during ozone depletion events,
353 Environ. Chem., 4, 238, 2007a.

354 Morin, S., Savarino, J., Bekki, S., Gong, S., and Bottenheim, J. W.: Signature of Arctic surface ozone depletion events in the
355 isotope anomaly ($\Delta^{17}\text{O}$) of atmospheric nitrate, Atmos. Chem. Phys., 7, 1451-1469, 2007b.

356 Morin, S., Savarino, J., Frey, M. M., Yan, N., Bekki, S., Bottenheim, J. W., and Martins, J. M.: Tracing the origin and fate of
357 NO_x in the Arctic atmosphere using stable isotopes in nitrate, Science, 322, 730-732, 2008.

358 Morin, S., Savarino, J., Frey, M. M., Domine, F., Jacobi, H. W., Kaleschke, L., and Martins, J. M.: Comprehensive isotopic
359 composition of atmospheric nitrate in the Atlantic Ocean boundary layer from 65 S to 79 N, J. Geophys. Res. Atmos.,
360 114, 2009.

361 Morin, S., Sander, R., and Savarino, J.: Simulation of the diurnal variations of the oxygen isotope anomaly ($\Delta^{17}\text{O}$) of reactive
362 atmospheric species, Atmos. Chem. Phys., 11, 3653-3671, 2011.

363 Nelson, D. M., Tsunogai, U., Ding, D., Ohyama, T., Komatsu, D. D., Nakagawa, F., Noguchi, I., and Yamaguchi, T.: Triple
364 oxygen isotopes indicate urbanization affects sources of nitrate in wet and dry atmospheric deposition, Atmos. Chem.
365 Phys., 18, 6381-6392, 2018.

366 Pathak, R. K., Wu, W. S., and Wang, T.: Summertime PM_{2.5} ionic species in four major cities of China: nitrate formation in
367 an ammonia-deficient atmosphere, Atmos. Chem. Phys., 9, 1711-1722, 2009.

368 Pathak, R. K., Wang, T., and Wu, W. S.: Nighttime enhancement of PM_{2.5} nitrate in ammonia-poor atmospheric conditions in
369 Beijing and Shanghai: plausible contributions of heterogeneous hydrolysis of N₂O₅ and HNO₃ partitioning, Atmos.
370 Environ., 45, 1183-1191, 2011.

371 Patris, N., Cliff, S. S., Quinn, P. K., Kasem, M., and Thiemens, M. H.: Isotopic analysis of aerosol sulfate and nitrate during
372 ITCT - 2k2: Determination of different formation pathways as a function of particle size, J. Geophys. Res. Atmos., 112,
373 2007.

374 Rao, Z., Chen, Z., Liang, H., Huang, L., and Huang, D.: Carbonyl compounds over urban Beijing: Concentrations on haze
375 and non-haze days and effects on radical chemistry, Atmos. Environ., 124, 207-216, 2016.

376 Savarino, J., and Thiemens, M. H.: Analytical procedure to determine both $\delta^{18}\text{O}$ and $\delta^{17}\text{O}$ of H₂O₂ in natural water and first
377 measurements, Atmos. Environ., 33, 3683-3690, 1999.

378 Savarino, J., Kaiser, J., Morin, S., Sigman, D. M., and Thiemens, M. H.: Nitrogen and oxygen isotopic constraints on the
379 origin of atmospheric nitrate in coastal Antarctica, Atmos. Chem. Phys., 7, 1925-1945, 2007.

380 Savarino, J., Bhattacharya, S. K., Morin, S., Baroni, M., and Doussin, J.-F.: The NO + O₃ reaction: A triple oxygen isotope
381 perspective on the reaction dynamics and atmospheric implications for the transfer of the ozone isotope anomaly, J.
382 Chem. Phys., 128, 194303, 2008.

383 Savarino, J., Morin, S., Erbland, J., Grannec, F., Patey, M. D., Vicars, W., Alexander, B., and Achterberg, E. P.: Isotopic
384 composition of atmospheric nitrate in a tropical marine boundary layer, *P. Natl. Acad. Sci. USA*, 110, 17668-17673,
385 2013.

386 Sofen, E. D., Alexander, B., Steig, E. J., Thiemens, M. H., Kunasek, S. A., Amos, H. M., Schauer, A. J., Hastings, M. G.,
387 Bautista, J., and Jackson, T. L.: WAIS Divide ice core suggests sustained changes in the atmospheric formation
388 pathways of sulfate and nitrate since the 19th century in the extratropical Southern Hemisphere, *Atmos. Chem. Phys.*,
389 14, 5749-5769, 2014.

390 Su, X., Tie, X., Li, G., Cao, J., Huang, R., Feng, T., Long, X., and Xu, R.: Effect of hydrolysis of N_2O_5 on nitrate and
391 ammonium formation in Beijing China: WRF-Chem model simulation, *Sci. Total Environ.*, 579, 221-229, 2017.

392 Sun, Y., Zhuang, G., Tang, A., Wang, Y., and An, Z.: Chemical characteristics of $PM_{2.5}$ and PM_{10} in haze-fog episodes in
393 Beijing, *Environ. Sci. Technol.*, 40, 3148-3155, 2006.

394 Tong, S., Hou, S., Zhang, Y., Chu, B., Liu, Y., He, H., Zhao, P., and Ge, M.: Comparisons of measured nitrous acid (HONO)
395 concentrations in a pollution period at urban and suburban Beijing, in autumn of 2014, *Sci. China Chem.*, 58,
396 1393-1402, 2015.

397 Tsunogai, U., Komatsu, D. D., Daita, S., Kazemi, G. A., Nakagawa, F., Noguchi, I., and Zhang, J.: Tracing the fate of
398 atmospheric nitrate deposited onto a forest ecosystem in Eastern Asia using $\Delta^{17}O$, *Atmos. Chem. Phys.*, 10, 1809-1820,
399 2010.

400 Tsunogai, U., Miyauchi, T., Ohyama, T., Komatsu, D. D., Nakagawa, F., Obata, Y., Sato, K., and Ohizumi, T.: Accurate and
401 precise quantification of atmospheric nitrate in streams draining land of various uses by using triple oxygen isotopes as
402 tracers, *Biogeosciences*, 13, 3441-3459, 2016.

403 Vicars, W. C., Morin, S., Savarino, J., Wagner, N. L., Erbland, J., Vince, E., Martins, J. M. F., Lerner, B. M., Quinn, P. K.,
404 and Coffman, D. J.: Spatial and diurnal variability in reactive nitrogen oxide chemistry as reflected in the isotopic
405 composition of atmospheric nitrate: Results from the CalNex 2010 field study, *J. Geophys. Res. Atmos.*, 118, 2013.

406 Vicars, W. C., and Savarino, J.: Quantitative constraints on the ^{17}O -excess ($\Delta^{17}O$) signature of surface ozone: Ambient
407 measurements from 50°N to 50°S using the nitrite-coated filter technique, *Geochim. Cosmochim. Acta*, 135, 270-287,
408 2014.

409 Walters, W. W., Simonini, D. S., and Michalski, G.: Nitrogen isotope exchange between NO and NO_2 and its implications for
410 $\delta^{15}N$ variations in tropospheric NO_x and atmospheric nitrate, *Geophys. Res. Lett.*, 43, 440-448, 2016.

411 Wang, D., Hu, R., Xie, P., Liu, J., Liu, W., Qin, M., Ling, L., Zeng, Y., Chen, H., Xing, X., Zhu, G., Wu, J., Duan, J., Lu, X.,
412 and Shen, L.: Diode laser cavity ring-down spectroscopy for in situ measurement of NO_3 radical in ambient air, *J. Quant.*
413 *Spectrosc. Radiat. Transf.*, 166, 23-29, 2015.

414 Wang, H., Chen, J., and Lu, K.: Development of a portable cavity-enhanced absorption spectrometer for the measurement of

415 ambient NO_3 and N_2O_5 : experimental setup, lab characterizations, and field applications in a polluted urban
416 environment, *Atmos. Meas. Tech.*, 10, 1465, 2017a.

417 Wang, H., Lu, K., Chen, X., Zhu, Q., Chen, Q., Guo, S., Jiang, M., Li, X., Shang, D., and Tan, Z.: High N_2O_5 concentrations
418 observed in urban Beijing: Implications of a large nitrate formation pathway, *Environ. Sci. Technol. Lett.*, 4, 416-420,
419 2017b.

420 Wang, H., Lu, K., Tan, Z., Sun, K., Li, X., Hu, M., Shao, M., Zeng, L., Zhu, T., and Zhang, Y.: Model simulation of NO_3 ,
421 N_2O_5 and ClNO_2 at a rural site in Beijing during CAREBeijing-2006, *Atmos. Res.*, 196, 97-107, 2017c.

422 Wang, H., Lu, K., Chen, X., Zhu, Q., Wu, Z., Wu, Y., and Sun, K.: Large particulate nitrate formation from N_2O_5 uptake in a
423 chemically reactive layer aloft during wintertime in Beijing, *Atmos. Chem. Phys. Discuss.*, 1-27, 2018a.

424 Wang, H., Lu, K., Guo, S., Wu, Z., Shang, D., Tan, Z., Wang, Y., Le Breton, M., Zhu, W., Lou, S., Tang, M., Wu, Y., Zheng,
425 J., Zeng, L., Hallquist, M., Hu, M., and Zhang, Y.: Efficient N_2O_5 Uptake and NO_3 Oxidation in the Outflow of Urban
426 Beijing, *Atmos. Chem. Phys. Discuss.*, 1-27, 2018b.

427 Wang, J., Zhang, X., Guo, J., Wang, Z., and Zhang, M.: Observation of nitrous acid (HONO) in Beijing, China: Seasonal
428 variation, nocturnal formation and daytime budget, *Sci. Total Environ.*, 587, 350-359, 2017d.

429 Wang, S., Zhang, Q., Streets, D. G., He, K., Martin, R. V., Lamsal, L. N., Chen, D., Lei, Y., and Lu, Z.: Growth in NO_x
430 emissions from power plants in China: bottom-up estimates and satellite observations, *Atmos. Chem. Phys.*, 12,
431 4429-4447, 2012.

432 Wang, Y., Zhou, L., Wang, M., and Zheng, X.: Trends of atmospheric methane in Beijing, *Chemosphere*, 3, 65-71, 2001.

433 Wen, L., Chen, J., Yang, L., Wang, X., Xu, C., Sui, X., Yao, L., Zhu, Y., Zhang, J., and Zhu, T.: Enhanced formation of fine
434 particulate nitrate at a rural site on the North China Plain in summer: The important roles of ammonia and ozone, *Atmos.*
435 *Environ.*, 101, 294-302, 2015.

436 Wu, R., Li, J., Hao, Y., Li, Y., Zeng, L., and Xie, S.: Evolution process and sources of ambient volatile organic compounds
437 during a severe haze event in Beijing, China, *Sci. Total Environ.*, 560, 62-72, 2016.

438 Xiao, H., Xie, L., Long, A., Ye, F., Pan, Y., Li, D., Long, Z., Chen, L., Xiao, H., and Liu, C.: Use of isotopic compositions of
439 nitrate in TSP to identify sources and chemistry in South China Sea, *Atmos. Environ.*, 109, 70-78, 2015.

440 Xu, X., Zhao, W., Zhang, Q., Wang, S., Fang, B., Chen, W., Venables, D. S., Wang, X., Pu, W., and Wang, X.: Optical
441 properties of atmospheric fine particles near Beijing during the HOPE-J3 A campaign, *Atmos. Chem. Phys.*, 16,
442 6421-6439, 2016.

443 Ye, P., Xie, Z., Yu, J., and Kang, H.: Spatial distribution of methanesulphonic acid in the Arctic aerosol collected during the
444 Chinese Arctic Research Expedition, *Atmosphere*, 6, 699-712, 2015.

445 Yu, Z., and Elliott, E. M.: Novel Method for Nitrogen Isotopic Analysis of Soil-Emitted Nitric Oxide, *Environ. Sci. Technol.*,
446 2017.

447 Zhang, J., Chen, Z., Lu, Y., Gui, H., Liu, J., Liu, W., Wang, J., Yu, T., Cheng, Y., and Chen, Y.: Characteristics of aerosol size
 448 distribution and vertical backscattering coefficient profile during 2014 APEC in Beijing, *Atmos. Environ.*, 148, 30-41,
 449 2017.

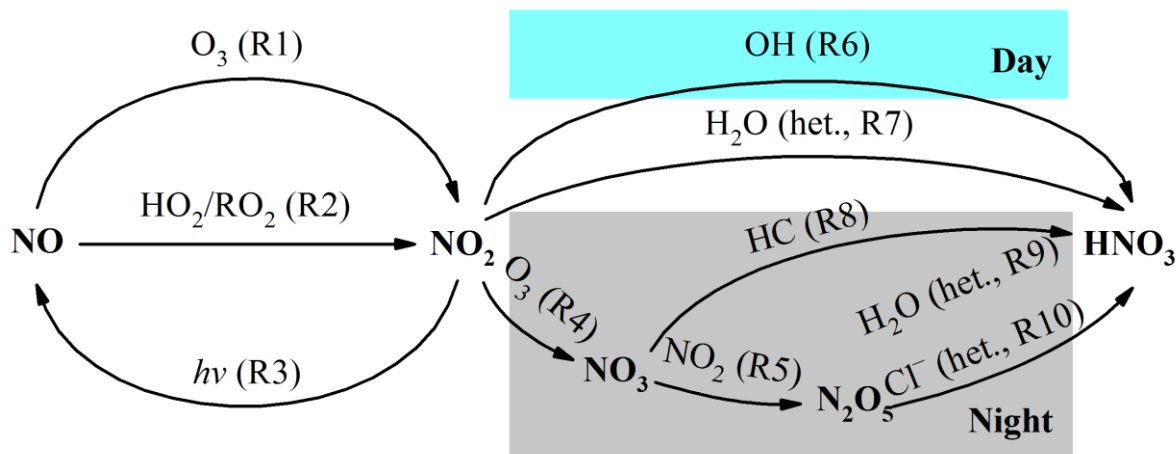
450 Zhang, Q., Streets, D. G., He, K., Wang, Y., Richter, A., Burrows, J. P., Uno, I., Jang, C. J., Chen, D., Yao, Z., and Lei, Y.:
 451 NO_x emission trends for China, 1995–2004: The view from the ground and the view from space, *J. Geophys. Res.*, 112,
 452 2007.

453 Zhang, Y., Liu, X., Fangmeier, A., Goulding, K. T. W., and Zhang, F.: Nitrogen inputs and isotopes in precipitation in the
 454 North China Plain, *Atmos. Environ.*, 42, 1436-1448, 2008.

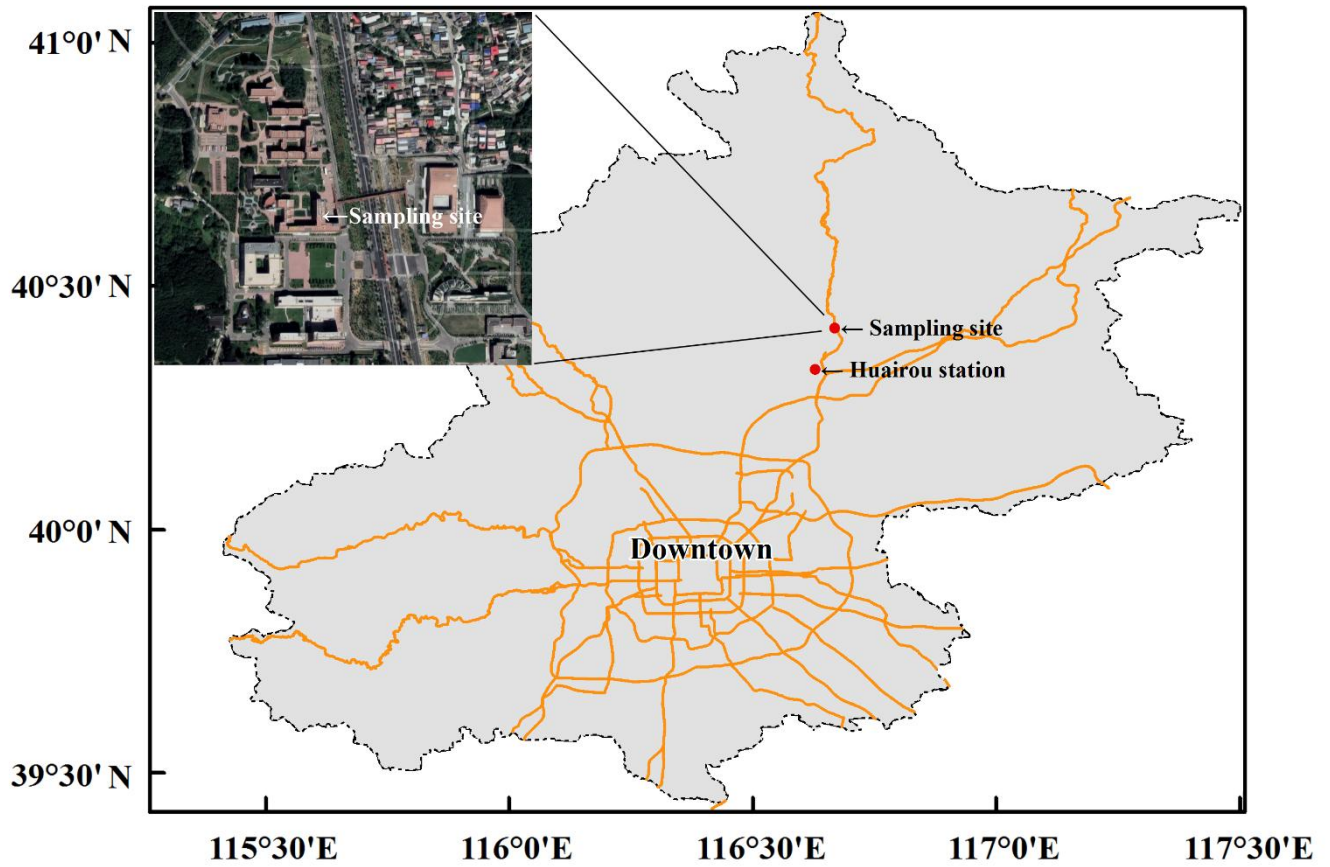
455 Zheng, B., Zhang, Q., Zhang, Y., He, K., Wang, K., Zheng, G., Duan, F., Ma, Y., and Kimoto, T.: Heterogeneous chemistry: a
 456 mechanism missing in current models to explain secondary inorganic aerosol formation during the January 2013 haze
 457 episode in North China, *Atmos. Chem. Phys.*, 15, 2031-2049, 2015a.

458 Zheng, G., Duan, F., Su, H., Ma, Y., Cheng, Y., Zheng, B., Zhang, Q., Huang, T., Kimoto, T., and Chang, D.: Exploring the
 459 severe winter haze in Beijing: the impact of synoptic weather, regional transport and heterogeneous reactions, *Atmos.*
 460 *Chem. Phys.*, 15, 2969-2983, 2015b.

461 **Figures and Tables**



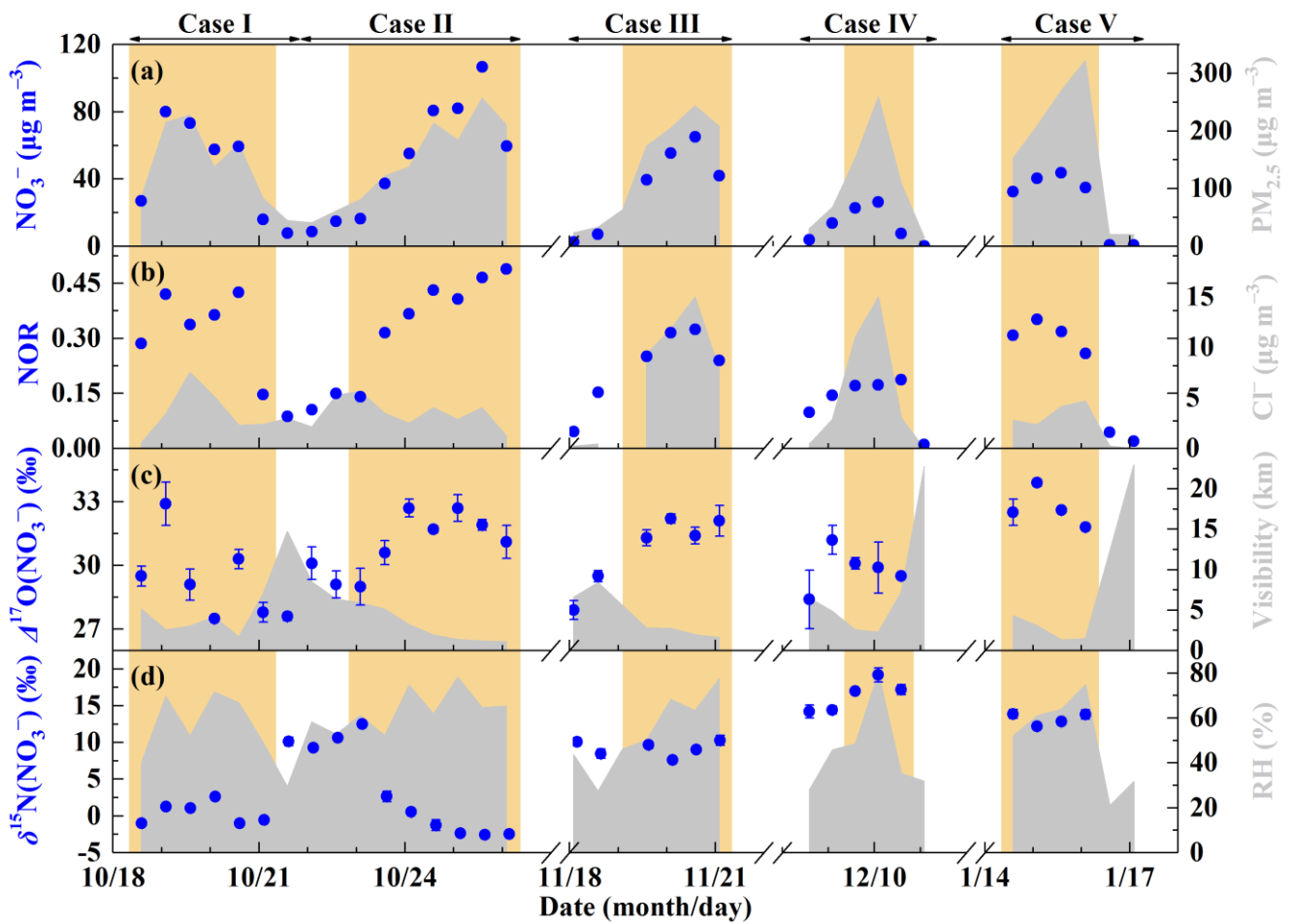
462
 463 **Figure 1.** Simplified schematic of the main nitrate formation pathways in urban air. “het.” means heterogeneous reactions on
 464 aerosols.



465

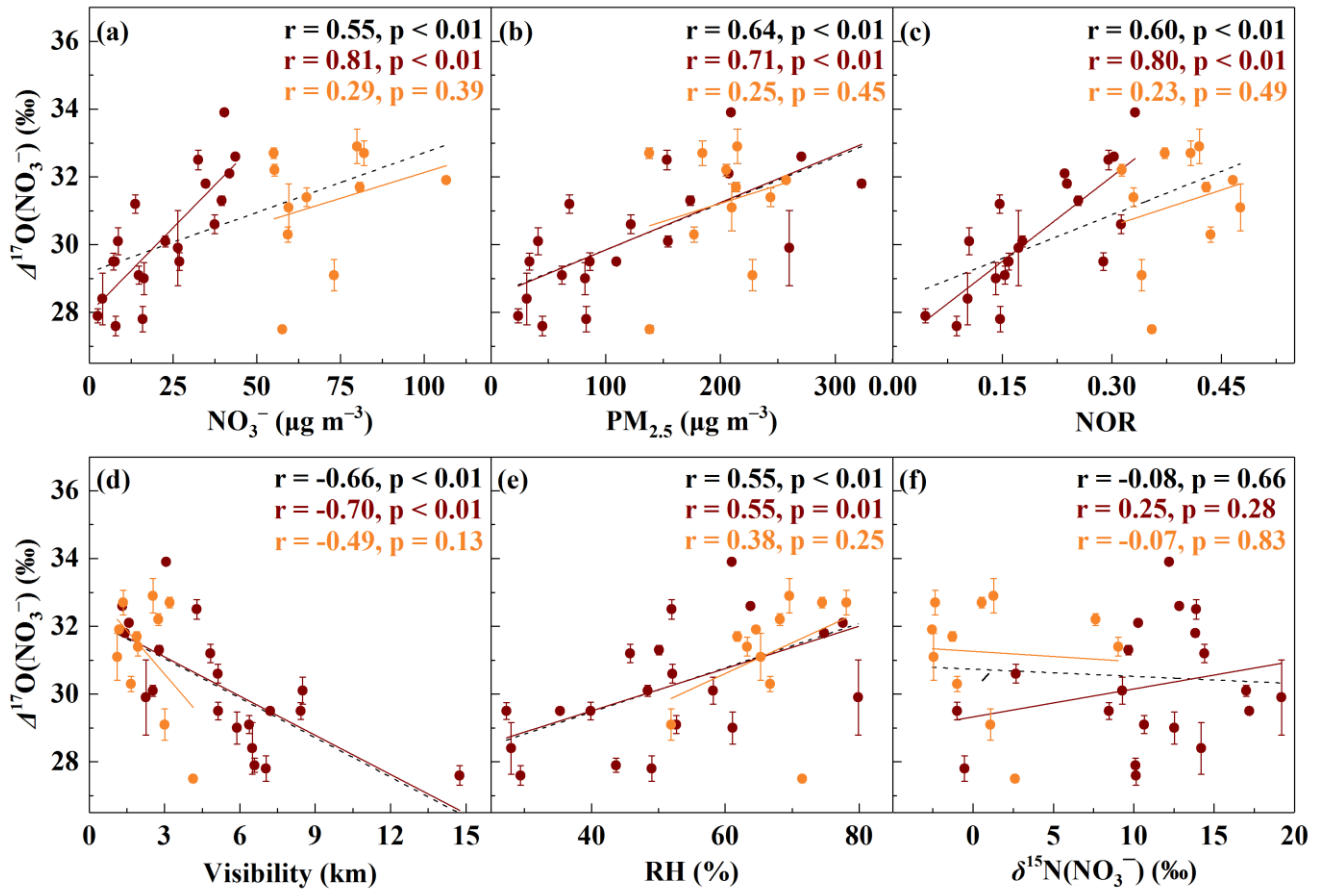
466 **Figure 2.** A brief map of sampling site in Beijing. The map scale of base map is 1:1250000. Huairou station is set by Beijing

467 Municipal Environmental Monitoring Center, where hourly $PM_{2.5}$, SO_2 , CO, NO_2 and O_3 were observed.



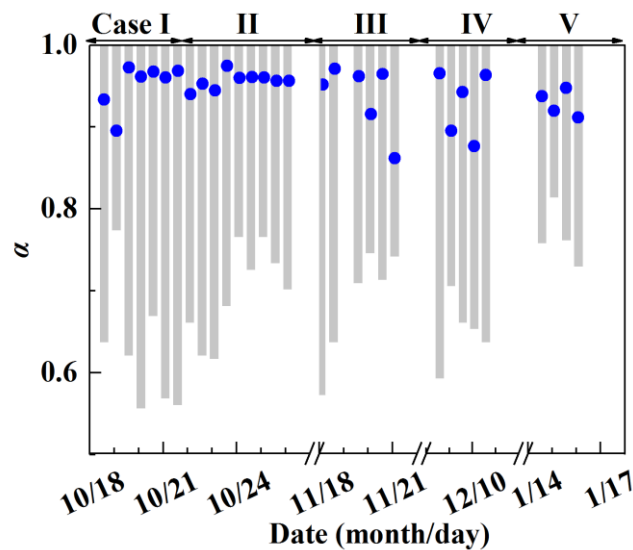
468

469 **Figure 3.** General characteristics of haze events in Beijing (October 2014 – January 2015). (a) Time series of PM_{2.5} and
 470 NO₃⁻ concentrations. (b) Time series of nitrogen oxidation ratio (NOR, which equals to NO₃⁻ molar concentration divided by
 471 the sum of NO₃⁻ and NO₂ molar concentration) and Cl⁻ concentrations. (c) Time series of Δ¹⁷O(NO₃⁻) and visibility. (d) Time
 472 series of δ¹⁵N(NO₃⁻) and relative humidity (RH). The error bars in (c) and (d) are ±1σ of replicate measurements (n = 3) of
 473 each sample. The khaki shaded area indicates polluted days (PD, PM_{2.5} ≥ 75 µg m⁻³).



474

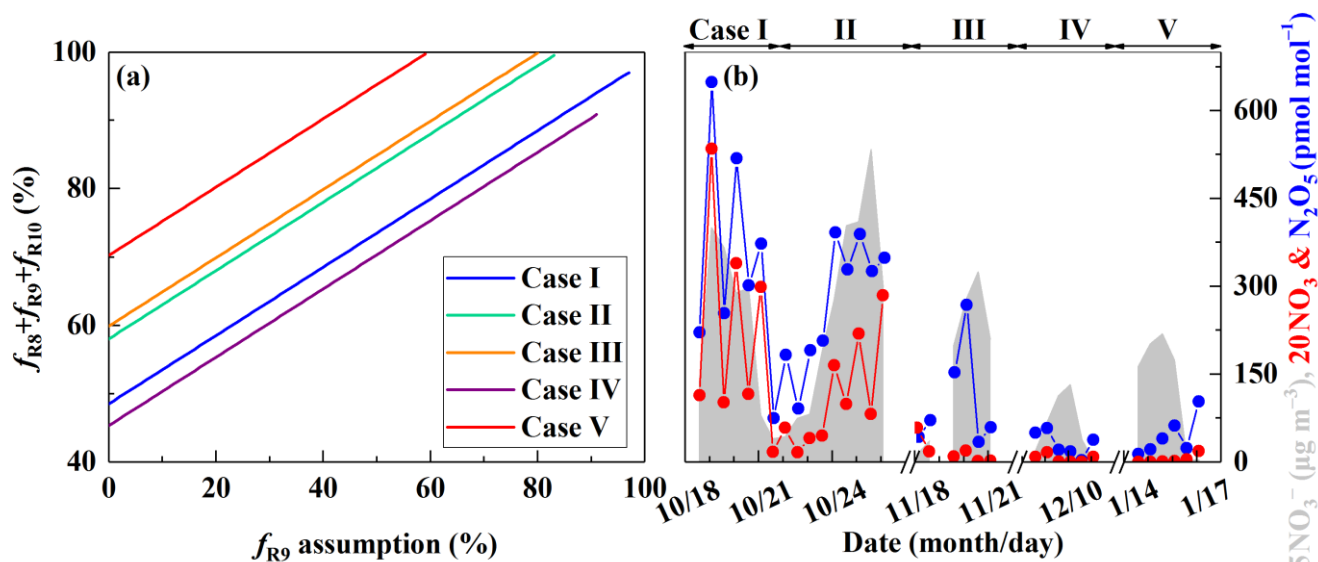
475 **Figure 4.** Relationships between $\Delta^{17}\text{O}(\text{NO}_3^-)$ and other parameters. The relationship between $\Delta^{17}\text{O}(\text{NO}_3^-)$ and NO_3^-
 476 concentrations (a), $\text{PM}_{2.5}$ concentrations (b), nitrogen oxidation ratio (NOR, c), visibility (d), relative humidity (RH, e) and
 477 $\delta^{15}\text{N}(\text{NO}_3^-)$ (f). The dark red dots are samples with $\text{NO}_3^- < 50 \mu\text{g m}^{-3}$ and the orange dots are samples with $\text{NO}_3^- > 50 \mu\text{g m}^{-3}$.
 478 The black dash lines are linear least-squares fitting lines for all samples, the dark red solid lines are linear least-squares
 479 fitting lines for samples with $\text{NO}_3^- < 50 \mu\text{g m}^{-3}$ and the orange solid lines are linear least-squares fitting lines for samples
 480 with $\text{NO}_3^- > 50 \mu\text{g m}^{-3}$. The error bars are $\pm 1\sigma$ of replicate measurements of each sample.



481

482 **Figure 5.** Estimate of the proportion of O_3 oxidation in NO_x cycling, α . The gray column represents possible α range

483 determined by $\Delta^{17}\text{O}(\text{NO}_3^-)$. The blue dot represents specific α value calculated by Eq. (3).



484
 485 **Figure 6.** Estimate of the nocturnal formation pathways. The estimated relative importance of nocturnal formation pathways
 486 ($f_{\text{R8}} + f_{\text{R9}} + f_{\text{R10}}$) during PD of each case on the basis of observed $\Delta^{17}\text{O}(\text{NO}_3^-)$ (See Sect. 2.3, a) and the simulated mixing
 487 ratios of N_2O_5 and NO_3 radical by MCM (b). R8, R9 and R10 in (a) represents $\text{NO}_3 + \text{HC}$, $\text{N}_2\text{O}_5 + \text{H}_2\text{O}$ and $\text{N}_2\text{O}_5 + \text{Cl}^-$
 488 pathway, respectively.

489 **Table 1.** Isotope assumptions of different nitrate formation pathways.

No.	Reaction	$\Delta^{17}\text{O}$ of product		Reference
		Expression	Value (‰) ^a	
R1	$\text{NO} + \text{O}_3 \rightarrow \text{NO}_2 + \text{O}_2$	$\Delta^{17}\text{O}(\text{NO}_2) = 1.18 \times \Delta^{17}\text{O}(\text{O}_3) + 6.6 \text{‰}$	37	(Savarino et al., 2008)
R2	$\text{NO} + \text{HO}_2/\text{RO}_2 \rightarrow \text{NO}_2 + \text{OH}/\text{RO}$	$\Delta^{17}\text{O}(\text{NO}_2) = 0.0$	0.0	(Sofen et al., 2014)
R4	$\text{NO}_2 + \text{O}_3 \rightarrow \text{NO}_3 + \text{O}_2$	$\Delta^{17}\text{O}(\text{NO}_3) =$ $\frac{2}{3}\Delta^{17}\text{O}(\text{NO}_2) + \frac{1}{3}(1.23 \times \Delta^{17}\text{O}(\text{O}_3) + 9.0 \text{‰})$	$25\alpha + 14$	(Berhanu et al., 2012)
R5	$\text{NO}_2 + \text{NO}_3 \rightarrow \text{N}_2\text{O}_5$	$\Delta^{17}\text{O}(\text{N}_2\text{O}_5) = \frac{2}{5}\Delta^{17}\text{O}(\text{NO}_2) + \frac{3}{5}\Delta^{17}\text{O}(\text{NO}_3)$	$30\alpha + 8$	(Sofen et al., 2014)
R6	$\text{NO}_2 + \text{OH} \rightarrow \text{HNO}_3$	$\Delta^{17}\text{O}(\text{NO}_3^-) = \frac{2}{3}\Delta^{17}\text{O}(\text{NO}_2)$	25α	(Sofen et al., 2014)
R7	$2\text{NO}_2 + \text{H}_2\text{O} \rightarrow \text{HNO}_3 + \text{HNO}_2$	$\Delta^{17}\text{O}(\text{NO}_3^-) = \frac{2}{3}\Delta^{17}\text{O}(\text{NO}_2)$	25α	^b
R8	$\text{NO}_3 + \text{HC} \rightarrow \text{HNO}_3 + \text{products}$	$\Delta^{17}\text{O}(\text{NO}_3^-) = \Delta^{17}\text{O}(\text{NO}_3)$	$25\alpha + 14$	(Sofen et al., 2014)
R9	$\text{N}_2\text{O}_5 + \text{H}_2\text{O} \rightarrow 2\text{HNO}_3$	$\Delta^{17}\text{O}(\text{NO}_3^-) = \frac{5}{6}\Delta^{17}\text{O}(\text{N}_2\text{O}_5)$	$25\alpha + 7$	(Sofen et al., 2014)
R10	$\text{N}_2\text{O}_5 + \text{Cl}^- \rightarrow \text{HNO}_3 + \text{ClNO}_2$	$\Delta^{17}\text{O}(\text{NO}_3^-) = \Delta^{17}\text{O}(\text{NO}_3)$	$25\alpha + 14$	^c

490 ^a The values are calculated on assumptions that bulk $\Delta^{17}\text{O}(\text{O}_3) = 26 \text{‰}$ (Vicars and Savarino, 2014; Ishino et al., 2017) and
 491 $\Delta^{17}\text{O}(\text{HO}_2/\text{RO}_2) = 0 \text{‰}$. $\Delta^{17}\text{O}(\text{RO}_2)$ is equal to 0‰ in the troposphere (Morin et al., 2011), in contrast, observations suggest
 492 $\Delta^{17}\text{O}(\text{HO}_2) = 1 - 2 \text{‰}$ (Savarino and Thiemens, 1999). However, the difference in calculated $\Delta^{17}\text{O}(\text{NO}_3^-)$ between assuming

493 $\Delta^{17}\text{O}(\text{HO}_2) = 0 \text{ ‰}$ and $\Delta^{17}\text{O}(\text{HO}_2) = 2 \text{ ‰}$ is negligible in this study ($< 0.1 \text{ ‰}$). And the assumption that $\Delta^{17}\text{O}(\text{HO}_2) = 0 \text{ ‰}$
 494 simplifies calculations and is also consistent with previous studies (Michalski et al., 2003; Alexander et al., 2009; Morin et
 495 al., 2008; Kunasek et al., 2008; Sofen et al., 2014). α is the proportion of O_3 oxidation in NO_2 production rate, calculated by
 496 Eq. (3).

497 ^b Previous studies suggest that in R7 one oxygen atom of NO_3^- is from H_2O and the other two are from NO_2 (Li et al., 2010;
 498 Cheung et al., 2000; Goodman et al., 1999), which will result in $\Delta^{17}\text{O}(\text{NO}_3^-) = 2/3\Delta^{17}\text{O}(\text{NO}_2)$.

499 ^c R4 and R5 suggest that the central oxygen atom of N_2O_5 ($\text{O}_2\text{N-O-NO}_2$) is from NO_3 radical (O-NO_2) with $\Delta^{17}\text{O} (\text{‰}) =$
 500 $1.23 \times \Delta^{17}\text{O}(\text{O}_3) + 9.0 \text{ ‰}$. R10 is suggested to occur via $\text{O}_2\text{N-O-NO}_2 (\text{aq}) \leftrightarrow \text{NO}_2^+ + \text{NO}_3^-$ and the following $\text{NO}_2^+ + \text{Cl}^- \rightarrow$
 501 ClNO_2 (Bertram and Thornton, 2009), so $\Delta^{17}\text{O}(\text{NO}_3^-) = 1/3(1.23 \times \Delta^{17}\text{O}(\text{O}_3) + 9.0 \text{ ‰}) + 2/3\Delta^{17}\text{O}(\text{NO}_2) = \Delta^{17}\text{O}(\text{NO}_3)$.

502 **Table 2.** Reaction expressions for different NO_2 production pathways.

No.	Reaction	Rate expression	Rate constant ($\text{cm}^3 \text{ molecule}^{-1} \text{ s}^{-1}$)	Reference
R1	$\text{NO} + \text{O}_3 \rightarrow \text{NO}_2 + \text{O}_2$	$k_{\text{R1}}[\text{NO}][\text{O}_3]$	$k_{\text{R1}} = 3.0 \times 10^{-12} \times e^{(-1500/T)}$	(Burkholder et al., 2015)
R2a	$\text{NO} + \text{HO}_2 \rightarrow \text{NO}_2 + \text{OH}$	$k_{2\text{Ra}}[\text{NO}][\text{HO}_2]$	$k_{2\text{Ra}} = 3.3 \times 10^{-12} \times e^{(270/T)}$	(Burkholder et al., 2015)
R2b	$\text{NO} + \text{RO}_2 \rightarrow \text{NO}_2 + \text{RO}$	$k_{2\text{Rb}}[\text{NO}][\text{RO}_2]$	$k_{2\text{Rb}} = k_{2\text{Ra}}$	(Burkholder et al., 2015; Kunasek et al., 2008)

503 **Table 3.** Atmospheric $\Delta^{17}\text{O}(\text{NO}_3^-)$ in aerosols obtained from the literature and this study.

Sample location	Sample period	Collection interval	$\Delta^{17}\text{O} (\text{‰})$ range	Reference
Huairou, Beijing (40.41 °N, 116.68 °E)	October 2014 – January 2015	12 h	27.5 – 33.9 (30.6 ± 1.8)	This study
Trinidad Head, California (41.0 °N, 124.2 °W)	April – May 2002	1 – 4 days	20.1 – 27.5	(Patris et al., 2007)
La Jolla, California (32.7 °N, 117.2 °W)	March 1997 – April 1998	3 days	20 – 30.8	(Michalski et al., 2003)
Mt. Lulin, Taiwan (23.5 °N, 120.9 °E)	January – December 2010	1 day	2.7 – 31.4 (17 ± 7)	(Guha et al., 2017)
Cape Verde Island (16.9 °N, 24.9 °W)	July 2007 – May 2008	2 – 3 days	25.5 – 31.3	(Savarino et al., 2013)
Cruise in costal California (32.8 °N – 38.6 °N)	May – June 2010	2 – 22 h	19.0 – 29.2 (24.1 ± 2.2)	(Vicars et al., 2013)
Cruise from 65 °S to 79 °N	September – October 2006	1 – 4 days	Non-polar:	(Morin et al., 2009)

	April – May 2007		24 – 33	
	February – April 2006		Polar: 35 ± 2	
Alert, Nunavut (82.5 °N, 62.3 °W)	March – May 2004	3 – 4 days	29 – 35 (32.7 ± 1.8)	(Morin et al., 2007b)
Barrow, Alaska (71.3 °N, 156.9 °W)	March 2005	1 day	26 – 36	(Morin et al., 2007a)
Dumont d’Urville, Antarctic (66.7 °S, 140.0 °E)	January – December 2001	10 – 15 days	20.0 – 43.1	(Savarino et al., 2007)
Dumont d’Urville, Antarctic (66.7 °S, 140.0 °E)	January 2011 – January 2012	7 days	23.0 – 41.9	(Ishino et al., 2017)

504 **Table 4** The possible range of fractional contribution of different nitrate formation pathways during PD of each case
505 estimated on the basis of observed $\Delta^{17}\text{O}(\text{NO}_3^-)$ ^a.

PD of Case	f_{R9} assumption (%)	$f_{R8} + f_{R9} + f_{R10}$ (%)	$f_{R8} + f_{R10}$ (%)	$f_{R6} + f_{R7}$ (%)
I	0 – 97	49 – 97	0 – 49	3 – 51
II	0 – 83	58 – 100	17 – 58	0 – 42
III	0 – 80	60 – 100	20 – 60	0 – 40
IV	0 – 90	45 – 90	0 – 45	10 – 55
V	0 – 59	70 – 100	41 – 70	0 – 30
Average	0 – 82	56 – 97	16 – 56	3 – 44

506 ^a R6, R7, R8, R9 and R10 is respectively $\text{NO}_2 + \text{OH}$, $\text{NO}_2 + \text{H}_2\text{O}$, $\text{NO}_3 + \text{HC}$, $\text{N}_2\text{O}_5 + \text{H}_2\text{O}$ and $\text{N}_2\text{O}_5 + \text{Cl}^-$ pathway.